Supercurrent reversal in Josephson junctions based on bilayer graphene flakes

Babak Zare Rameshti, Malek Zareyan,* and Ali G. Moghaddam
Department of Physics, Institute for Advanced Studies in Basic Sciences (IASBS), Zanjan 45137-66731, Iran
(Received 17 March 2015; revised manuscript received 25 May 2015; published 5 August 2015)

We investigate the Josephson effect in a bilayer graphene flake contacted by two monolayer sheets deposited by superconducting electrodes. It is found that when the electrodes are attached to the different layers of the bilayer, the Josephson current is in a π state, if the bilayer region is undoped and there is no vertical bias. Applying doping or bias to the junction reveals $\pi - 0$ transitions which can be controlled by varying the temperature and the junction length. The supercurrent reversal here is very different from the ferromagnetic Josephson junctions where the spin degree of freedom plays the key role. We argue that the scattering processes accompanied by layer and sublattice index change give rise to the scattering phases, the effect of which varies with doping and bias. Such scattering phases are responsible for the $\pi - 0$ transitions. On the other hand, if both of the electrodes are coupled to the same layer of the flake or the flake has AA stacking instead of common AB, the junction will be always in 0 state since the layer or sublattice index is not changed.

DOI: 10.1103/PhysRevB.92.085403 PACS number(s): 72.80.Vp, 74.50.+r, 74.45.+c, 85.25.Cp

I. INTRODUCTION

Starting from a decade ago, two-dimensional (2D) atomic layers were synthesized and received a huge amount of interest [1]. Graphene, the leading 2D material, has been studied a lot, mostly because of promising applications in electronics, chemistry, optics, etc., aside from the unexpected, relativisticlike electronic dispersion sparking interest from a fundamental point of view [2]. It has been shown that although the low-energy quasiparticles in single-layer graphene are massless Dirac fermions, however, the situation for bilayer graphene (BG) is fundamentally different, revealing chiral gapless excitations with quadratic dispersion rather than linear [3–5]. Subsequently, the electronic properties of mono- and bilayer graphene differ significantly from each other, the most famous example being, due to the so-called Klein tunneling, in monolayer graphene (MG) the backscattering is absent, while in the case of bilayer, the forward scattering is impossible [6]. Very intriguingly one can simply use a perpendicular electric field to generate a controllable gap in graphene bilayers [7–12].

Recently, it has been experimentally revealed that in epitaxial graphene, it is very probable to have steplike monolayer/bilayer (ML/BL) interfaces as well as bilayer flakes connected to monolayer regions [13–15]. A natural question arises immediately about the interplay of massless and massive dispersions in the junctions containing both mono- and bilayer graphene regions. Earlier theoretical investigations had proven that in the ML/BL interfaces the transmission probabilities can show a valley-dependent asymmetry, which suggests their usage in the generation of valley-polarized electron beams [16–18]. Moreover, in the presence of perpendicular magnetic fields the emergence of Landau levels with peculiar transport properties has been studied [19–22]. In particular, a rich Landau spectrum has been predicted [19] and an asymmetry in the dependence of transport features to the sign of magnetic field and charge carriers has been experimentally observed [20]. Other theoretical works have focused on the edge-state properties and quantum transport via channels introduced by the interface [23–29]. On the other hand, theoretical investigations of the transport through a bilayer flake sandwiched between two monolayer nanoribbons have revealed that the conductance oscillates between maximum and zero as a function of bilayer flake length [30].

The pioneering work of Beenakker [31,32] and successive experimental realization of the superconducting proximity effect and supercurrent passing through graphene [33] proved that graphene-based superconducting heterostructures can have very interesting properties [34–42], some of which are experimentally realized [43–48]. Among the variety of theoretical predictions, the so-called specular Andreev reflection, despite several proposals, still waits to be detected [49–52]. In addition, when the normal graphene region is replaced with a magnetic region, the well-known $0 - \pi$ transitions have been predicted to take place with some features different from conventional superconductor-ferromagnet-superconductor (SFS) junctions [53–55]. Intriguingly, it has been suggested that one can see the transitions by varying the doping of the magnetic region sandwiched between superconductors [56,57].

In this paper we investigate the Josephson effect through a BG flake embedded between two monolayer sheets, as can be seen in Fig. 1. We find that the first setup, in which the two ML leads are coupled to the lower and upper layers of the flake, is in the Josephson π state when the doping μ and vertical bias V_0 are zero. By applying gate voltages, which results in doping, and bias to the flake the device can undergo a π to 0 transition. Moreover, at the presence of finite μ or V_0, the $0 - \pi$ transitions occur with temperature and junction length as well. It must be noted that the reason for such transitions are in contrast with those taking place in the Josephson devices with ferromagnetic weak links. Here the origin of the π state is the phase factors of transmission coefficients through the flake which influence the superconducting phase dependence of the current carrying Andreev bound states. The appearance of phases is somehow related to the fact that quasiparticles passing through the flake in setup (a) need to change their layer and sublattice index, while in setup (b) for all the modes the scattering phases are zero. Varying the bias voltage and doping of the flake changes the scattering properties of the flake and at certain points the overall effects of the scattering

*Deceased 24 Feb 2014.

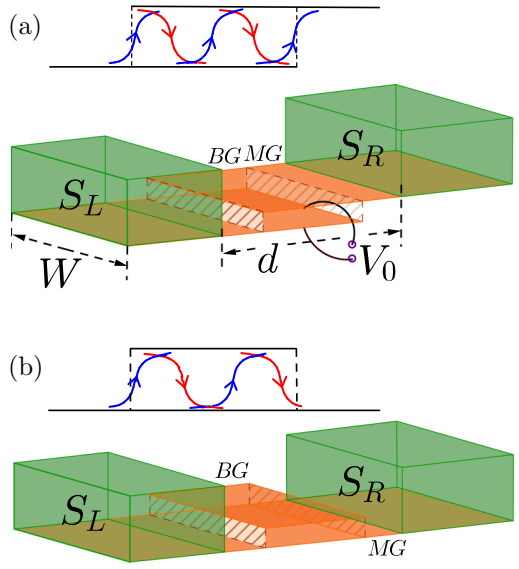

FIG. 1. (Color online) Josephson couplings. Supercurrent streams through the biased BG flakes embedded between two Josephson coupled superconducting MG leads, S_L and S_R. The length and width of the junction is indicated by d and W, respectively. A voltage difference V_0 is applied perpendicularly between the BG layers. The two superconductors are either (a) attached to the top and bottom layer of the BG flake, respectively, or (b) connected to only one particular layer of the bilayer. A qualitative description in the top of each setup demonstrates the transmission of the quasiparticles through the BG flakes by the red and blue curved arrows.

phases are diminished, leading to the 0 state Josephson effect.

This article is organized as follows. In Sec. II we introduce our model and explain the method we use to calculate the supercurrent that streams between two Josephson coupled superconducting leads. In Sec. III we present and discuss our numerical results that show the effect due to the bilayer step junction, as well as the effect of bias voltage on supercurrent. Finally, in Sec. IV we conclude and summarize our main findings.

II. MODEL AND BASIC FORMALISM

We investigate the supercurrent flowing between two superconducting reservoirs on top of MG regions which are connected through a weak link containing a biased BG flake. In fact, there are two different configurations for the setup depending on how the BG flake is connected to the MG regions in the left and right [58]. The left and right reservoirs can be attached to the top and bottom layers of the bilayer, respectively, as Fig. 1(a), or both of the monolayer reservoirs are connected to the same layer of the flake as Fig. 1(b). To be precise, we will assume the MG regions are fully covered by superconductors and only the middle BG flake is in the normal state.

We assume that the monolayer graphene regions which are underneath the superconducting leads become superconducting due to the fact that they are heavily doped. As a result, the Fermi wavelength λ_{FS} inside them is much smaller than the superconducting coherence length ξ and also the Fermi wavelength of the normal region λ_{FN}. By this condition the mean-field theory of superconductivity will be justified, and in addition, we can neglect the spatial variation of the superconducting order parameter $\Delta(\mathbf{r})$ inside the superconductors close to the normal superconducting (NS) interfaces [31]. Thus the superconducting order parameter has the constant values $\Delta(\mathbf{r}) = \Delta_0 e^{i\phi_{L,R}}$ in the left and right superconductor, respectively, and vanishes identically in N, where Δ_0 is the amplitude of an isotropic s-wave pairing.

Similar to any other weak link, the supercurrent across the junction is mainly carried by the discrete bound states which are the result of closed loop motion of the quasiparticles with subgap energies between two superconductors, known as the Andreev bound states (ABS). One can see that it is usually sufficient to find ABS energies in order to calculate the supercurrent carried by them. In the short junction limit, where the length of the junction (d) is much smaller than the coherence length of the superconductor (ξ), the current established due to the phase dependence of ABS energies and the continuous spectrum does not contribute since its density of states is almost phase independent. The relation between the Josephson current I passing through the junction with the transverse width W and subgap quasiparticles (ε_n) at finite temperature T is given by

$$I = -\frac{2eW}{\hbar}\int dk_y \sum_n \tanh\left[\frac{\varepsilon_n(k_y)}{2k_BT}\right]\frac{d\varepsilon_n(k_y)}{d\phi}. \qquad (1)$$

The sum is over all ABS energies, which are positive corresponding to the different transverse momenta k_y.

The ABS energies can be calculated in the framework of Bogoliubov–de Gennes (BdG) equations which describe the superconducting correlations between particles and their time-reversed counterparts (holes). For this excitation, it reads [31]

$$\begin{pmatrix} H_{MG} & \Delta(\mathbf{r}) \\ \Delta^*(\mathbf{r}) & -\Theta H_{MG}\Theta^{-1} \end{pmatrix}\begin{pmatrix}\psi_e \\ \psi_h\end{pmatrix} = \varepsilon\begin{pmatrix}\psi_e \\ \psi_h\end{pmatrix}, \qquad (2)$$

where H_{MG} is the single-particle Dirac Hamiltonian of the MG, which will be provided in the following section, and Θ is the time-reversal operator. The coherence factor of the BCS theory ψ_e, which consists of two components corresponding to the two sublattices, characterizes the particle part of the total wave function while the spinor $\psi_h = \Theta\psi_e$ describes the hole part of it.

Exploiting the BdG equations, the ABS energies will be obtained as the roots of a characteristic equation containing the whole scattering matrix of the junction. This method is based on the fact that the ABS can be assumed, as the states scattered completely to themselves inside the junction. The whole scattering matrix consists of two parts: S_B, which describes the normal scatterings of electrons and holes within the bilayer flake, and S_A, responsible for the scattering away from the normal-superconducting (NS) interfaces. Since for subgap energies $\varepsilon < \Delta_0$ there are no propagating modes in the superconducting regions L and R, then the scattering matrix S_A can be defined with relation $a_B = S_A b_B$, which relates the outgoing to incoming quasiparticles. This matrix consists of four blocks in electron-hole (Nambu) space corresponding to

different processes as

$$\mathrm{S}_A = \begin{pmatrix} \check{\mathrm{S}}_{ee} & \check{\mathrm{S}}_{eh} \\ \check{\mathrm{S}}_{he} & \check{\mathrm{S}}_{hh} \end{pmatrix}. \tag{3}$$

In general, each block of the scattering matrix in Nambu space denoted by $\check{\mathrm{S}}$ has the following form:

$$\check{\mathrm{S}} = \begin{pmatrix} \hat{r}_{LL} & \hat{t}_{LR} \\ \hat{t}_{RL} & \hat{r}_{RR} \end{pmatrix}, \tag{4}$$

consisting of reflection $\hat{r}$ and transmission $\hat{t}$ matrices which here are 2×2 matrices in the space of two layers. The scattering matrix of the NS interfaces involves only the reflection processes, and subsequently the corresponding normal and Andreev reflection parts are block diagonal as follows:

$$\check{\mathrm{S}}_{ee} = \begin{pmatrix} \hat{\mathrm{S}}^L_{ee} & 0 \\ 0 & \hat{\mathrm{S}}^R_{ee} \end{pmatrix}, \ \check{\mathrm{S}}_{eh} = \begin{pmatrix} \hat{\mathrm{S}}^L_{eh} & 0 \\ 0 & \hat{\mathrm{S}}^R_{eh} \end{pmatrix}. \tag{5}$$

Remember that at the left and right NS interfaces, depending on the configuration, either different layers [setup (a) in Fig. 1] or only one of the layers [setup (b) in Fig. 1] are involved in the reflection processes. As a result, the matrices for the two setups are respectively obtained as

$$\begin{aligned} &(a): \\ &\hat{\mathrm{S}}^L_{ee} = -\alpha(\varepsilon)\hat{\tau}_u \ , \ \hat{\mathrm{S}}^L_{eh} = \beta(\varepsilon)e^{i\phi/2}\hat{\tau}_u, \\ &\hat{\mathrm{S}}^R_{ee} = \alpha(\varepsilon)\hat{\tau}_d \ , \ \hat{\mathrm{S}}^R_{eh} = \beta(\varepsilon)e^{-i\phi/2}\hat{\tau}_d, \end{aligned} \tag{6}$$

$$\begin{aligned} &(b): \\ &\hat{\mathrm{S}}^L_{ee} = -\alpha(\varepsilon)\hat{\tau}_u \ , \ \hat{\mathrm{S}}^L_{eh} = \beta(\varepsilon)e^{i\phi/2}\hat{\tau}_u, \\ &\hat{\mathrm{S}}^R_{ee} = \alpha(\varepsilon)\hat{\tau}_u \ , \ \hat{\mathrm{S}}^R_{eh} = \beta(\varepsilon)e^{-i\phi/2}\hat{\tau}_u, \end{aligned} \tag{7}$$

with $\hat{\tau}_{u,d} = (\hat{\tau}_0 \pm \hat{\tau}_z)/2$, in which $\hat{\tau}_i$ are the Pauli matrices in the layer space and $\check{\mathrm{S}}_{hh} = -\check{\mathrm{S}}_{ee}$, $\hat{\mathrm{S}}^L_{he} = \exp(-i\phi)\hat{\mathrm{S}}^L_{eh}$, $\hat{\mathrm{S}}^R_{he} = \exp(i\phi)\hat{\mathrm{S}}^R_{eh}$. The normal and Andreev reflection amplitudes are obtained for the MG-based NS interfaces from matching the states in the N and S regions, by demanding continuity at the boundaries (see Ref. [31]), as $\alpha(\varepsilon) = i\zeta \sin\theta/[(\varepsilon/\Delta_0)\cos\theta + \zeta]$ and $\beta(\varepsilon) = \cos\theta/[(\varepsilon/\Delta_0)\cos\theta + \zeta]$, in which $\zeta = \sqrt{(\varepsilon/\Delta_0)^2 - 1}$ and θ is the incidence angle.

The scattering matrix of the normal BG region S_B relates two coefficient vectors, transmitted and reflected, as $b_B = \mathrm{S}_B a_B$. Owing to the fact that matrix S_B does not couple the electrons and holes together, it has a block-diagonal form given by

$$\mathrm{S}_B = \begin{pmatrix} \hat{\mathrm{S}}(\varepsilon) & 0 \\ 0 & \hat{\mathrm{S}}^*(-\varepsilon) \end{pmatrix}. \tag{8}$$

Here $\mathrm{S}(\varepsilon)$ and $\mathrm{S}^*(-\varepsilon)$ are the unitary and symmetric scattering matrices governing the scattering properties of the electrons and holes. The reflection and transmission matrices $\hat{r}$ and $\hat{t}$ for the BG flake embedded between two MG are given by

$$\begin{aligned} &(a): \\ &\hat{r}_{LL} = r_{11}\hat{\tau}_u \ , \ \hat{r}_{RR} = r^{'}_{22}\hat{\tau}_d \\ &\hat{t}_{LR} = t^{'}_{12}\hat{\tau}_+ \ , \ \hat{t}_{RL} = t_{21}\hat{\tau}_- \end{aligned} \tag{9}$$

$$\begin{aligned} &(b): \\ &\hat{r}_{LL} = r_{11}\hat{\tau}_u \ , \ \hat{r}_{RR} = r^{'}_{11}\hat{\tau}_u \\ &\hat{t}_{LR} = t^{'}_{11}\hat{\tau}_u \ , \ \hat{t}_{RL} = t_{11}\hat{\tau}_u \end{aligned} \tag{10}$$

for the two different setups, respectively, with $\hat{\tau}_\pm = (\hat{\tau}_x \pm i\hat{\tau}_y)/2$. The labels 1 and 2 denote the two layers of the BG flake. Therefore it is clear from above relations that in setup (b) the layer index is conserved, however, in the setup (a), since the only way to pass through the scattering region is via the interlayer hopping between the two layers where it is not conserved anymore. Transmission t_{ij} and reflection r_{ij} amplitudes can be obtained by matching the wave functions at the ML/BL boundaries. In order to complete the construction of the layer-resolved scattering matrix, the excitation spectrum of BG as well as MG and their wave functions as the scattering basis are needed.

The low-energy Hamiltonian of the BG flake in the presence of layer asymmetry due to the bias voltage applied perpendicularly and in the vicinity of nonequivalent corners of Brillouin zone K and K' is given by

$$\mathcal{H}_{\mathrm{BG}} = \begin{pmatrix} -\mu + \frac{V}{2} & v_F p_- & t_\perp & 0 \\ v_F p_+ & -\mu + \frac{V}{2} & 0 & 0 \\ t_\perp & 0 & -\mu - \frac{V}{2} & v_F p_+ \\ 0 & 0 & v_F p_- & -\mu - \frac{V}{2} \end{pmatrix}, \tag{11}$$

in the layer and sublattice spaces, with eigenfunctions of the form $\Phi^\dagger_{\mathbf{p}} = (c_{A1,\mathbf{p}}, c_{B1,\mathbf{p}}, c_{B2,\mathbf{p}}, c_{A2,\mathbf{p}})$. Here $p_\pm = p_x \pm ip_y$ and $\mathbf{p} = (p_x, p_y)$ is the two-dimensional momentum measured relative to the K point, $v_F \approx 10^6 m/s$ is the Fermi velocity within a monolayer, and μ is the chemical potential. The nearest-neighbor atoms in two layers $A1$ and $B2$ are connected by an interlayer hopping term $t_\perp \simeq 0.3ev$, which tends to equalize the charge densities in the two layers. The potential difference between the two layers is involved by the parameter V, which opens a gap in the spectrum, in contrast to the case of a gapless spectrum with $V = 0$. The vertical bias through the BG also works against the interlayer hopping since it generates charge imbalance between the two layers. Taking a plane-wave basis, for the excitation spectrum of the Hamiltonian we end up with four energy bands given by

$$\begin{aligned} (\varepsilon_{\mathrm{BG}} + \mu)^2 = (v_F p)^2 + (V^2/4) + (t_\perp^2/2) \\ \pm \sqrt{(t_\perp^2/2)^2 + (v_F p)^2(V^2 + t_\perp^2)}, \end{aligned} \tag{12}$$

and the corresponding eigenvector reads

$$\Phi^\dagger_{\mathbf{p}} = \mathcal{A}\begin{pmatrix} \gamma_- & v_F p_+ & \eta & \frac{\eta}{\gamma_+} v_F p_- \end{pmatrix}, \tag{13}$$

where $\eta = [\gamma_-^2 - (v_F p)^2]/t_\perp$ with $\gamma_\pm = \varepsilon_{\mathrm{BG}} + \mu \pm V/2$ and the normalization factor is $\mathcal{A} = [4v_F p_x(\gamma_- - (\varepsilon_{\mathrm{BG}} + \mu)V\eta/\gamma_+)]^{-1/2}$.

In order to find the scattering matrix S_B we need the eigenfunctions inside the left and right MG regions which are immediately coupled to the superconductors. The wave functions are represented in the space of two sublattices as

$\Phi^{\dagger}_{\mathbf{k}} = (c_{A1,\mathbf{k}}, c_{B1,\mathbf{k}})$, and the two-dimensional Dirac Hamiltonian around K and K' points reads

$$\mathcal{H}_{\rm MG} = \begin{pmatrix} \mu' & v_F(k_x - ik_y) \\ v_F(k_x + ik_y) & \mu' \end{pmatrix}. \quad (14)$$

Here the two-dimensional momentum is $\mathbf{k} = (k_x, k_y)$ and μ' is the chemical potential in the MG so that the excitation energy given by $\varepsilon_{\rm MG} = \mu' \pm v_F k$ is measured with respect to the Fermi energy in MG. The corresponding eigenvectors are

$$\Phi^{\dagger}_{\mathbf{k},\xi} = (2\cos\theta)^{-1/2}(1 \quad e^{i\theta}), \quad (15)$$

with $\xi = L, R$ and $\theta = \arctan(k_y/k_x)$. Since the eigenvectors will be utilized as the scattering basis, they need to be normalized in such a way that each state carries the same amount of quasiparticle current density.

We are now in a position to write down the wave functions in the left, middle, and right region as a linear superposition of constructed scattering basis equations (13) and (15):

$$\begin{aligned} \Psi_L &= \Phi^{+}_{\mathbf{k},L} e^{i(k_x x + k_y y)} + r\Phi^{-}_{\mathbf{k},L} e^{i(-k_x x + k_y y)}, \\ \Psi_{\rm B} &= a\Phi^{+}_{\mathbf{p},1} e^{i(p_{1x} x + k_y y)} + b\Phi^{+}_{\mathbf{p},2} e^{i(p_{2x} x + k_y y)} \\ &\quad + c\Phi^{-}_{\mathbf{p},1} e^{i(-p_{1x} x + k_y y)} + d\Phi^{-}_{\mathbf{p},2} e^{i(-p_{2x} x + k_y y)}, \\ \Psi_R &= t\Phi^{+}_{\mathbf{k},R} e^{i(k_x (x-d) + k_y y)}, \end{aligned} \quad (16)$$

where $+(-)$ denotes the right (left) moving quasiparticles with r and t being the reflection and transmission amplitudes, respectively. Scattering coefficients can be computed by solving the linear system constructed from the matching boundary conditions at the interfaces and subsequently will be used to find the transport properties across the junction. Thus we need to provide the appropriate boundary conditions at the boundaries $x = 0$ and $x = d$. The MGs can be attached either to the same layer of BG or to the different layers. We assume the zigzag boundary conditions at the ML/BL interfaces. The boundary conditions at the left interface $x = 0$ are

$$\begin{aligned} &\Psi_L(x=0)\big|_{A_1} = \Psi_B(x=0)\big|_{A_1}, \\ &\Psi_L(x=0)\big|_{B_1} = \Psi_B(x=0)\big|_{B_1}, \\ &\Psi_B(x=0)|_{A_2} = 0, \end{aligned} \quad (17)$$

and for the setup (b) they will be similar at the right interface as well. However, considering the top layer as the connecting layer between the right lead and the scattering region [setup (a)], at the right interface $x = d$ we must have

$$\begin{aligned} &\Psi_R(x=d)\big|_{A_2} = \Psi_B(x=d)\big|_{A_2}, \\ &\Psi_R(x=d)\big|_{B_2} = \Psi_B(x=d)\big|_{B_2}, \\ &\Psi_B(x=d)|_{B_1} = 0. \end{aligned} \quad (18)$$

Having both scattering matrices $S_{\rm A}$ and $S_{\rm B}$, the general condition for bound states $a_B = {\rm S}_A {\rm S}_B a_B$ implies that $\det(1 - {\rm S}_A {\rm S}_B) = 0$. Subsequently, from Eqs. (3) and (8) we find the following characteristic equation for the ABS energies:

$$\begin{aligned} &\det\{1 - \check{\rm S}_{ee}[\hat{\rm S}(\varepsilon) - \hat{\rm S}^*(-\varepsilon)] - \check{\rm S}_{ee}\hat{\rm S}(\varepsilon)\check{\rm S}_{ee}\hat{\rm S}^*(-\varepsilon) \\ &\quad -[1 - \check{\rm S}_{ee}\hat{\rm S}(\varepsilon)]\check{\rm S}_{he}\hat{\rm S}(\varepsilon)[1 - \check{\rm S}_{ee}\hat{\rm S}(\varepsilon)]^{-1}\check{\rm S}_{eh}\hat{\rm S}^*(-\varepsilon)\} = 0, \end{aligned} \quad (19)$$

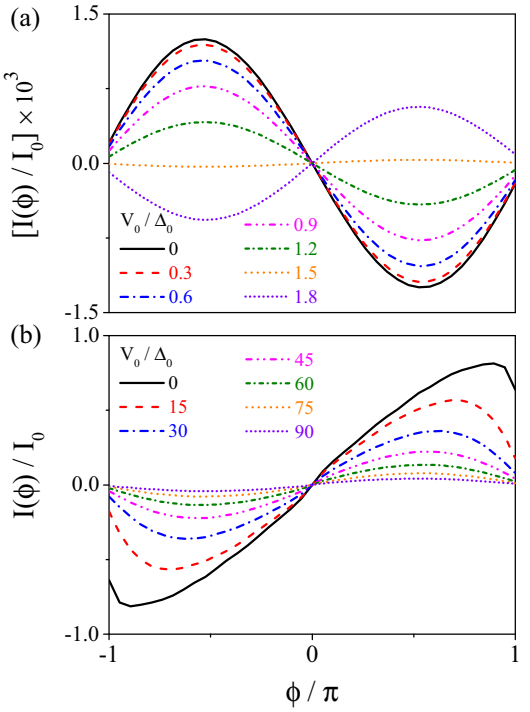

FIG. 2. (Color online) The current-phase relation $I(\phi)/I_0(T)$ in the short junctions made of undoped BG flakes are shown at zero temperature ($T = 0$), varying the scaled bias voltage V_0/Δ_0 for the first setup in (a) and for the second one in (b). The length of the junction is fixed at $d/l_\perp = 4$.

which can be used to find the Josephson current across the junction given by Eq. (1).

III. RESULTS AND DISCUSSION

Here the numerical results for the Josephson current passing through BG flakes between ML regions contacted by superconductors are presented. First we assume the undoped BG with $\mu = 0$ and study the current phase relation (CPR) by varying the vertical bias. We denote the Fermi wave vector inside the monolayer regions which are connected to the superconductors with k_F and define $l_\perp = \hbar v_F/t_\perp$, which is a length scale over which the excitations traveling in the two layers of the BG are coupled. Figure 2 shows the supercurrent variations $I(\phi)$ scaled by $I_0(T) = 4e\Delta(T)Wk_F/\hbar$ for the two different setups when the junction length is $d/l_\perp = 4$ and at the zero temperature $T = 0$. We see that in the absence of vertical bias V_0 the setup (a) is in the so-called π state with $I(\phi)/I_0 \sim \sin(\pi + \phi)$ while the other is in a 0 state, revealing a CPR of the form $I(\phi)/I_0 \sim \sin\phi$. Very intriguingly, when the vertical bias is applied the first setup can pass a $0 - \pi$ transition when $V_0 \sim 1.5\Delta_0$, as we see in Fig. 2(a). However, the second setup remains always in the 0 state, and increasing the vertical bias only suppresses the current. Moreover, we note that the amplitude of current in two cases is very different, and for the considered parameters, setup (b) has almost 3 orders of magnitude larger supercurrent.

It is worth noting that the main difference between two setups is the role of interlayer hopping $t_\perp$ in their transport

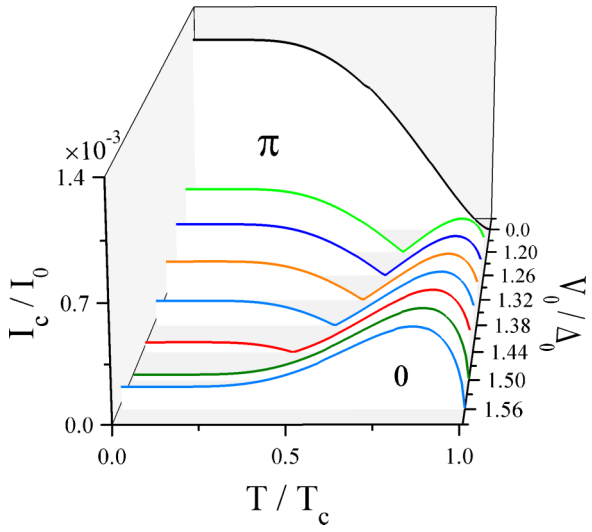

FIG. 3. (Color online) Critical current I_c/I_0 as a function of normalized temperature T/T_c depicted versus different values of scaled bias voltage $V_0/t_\perp$, shifted on the z axis, for setup (a). The dimensionless length of the junction is fixed at $d/l_\perp = 4$. The cusp in the curves represents the $\pi - 0$ transition where the critical current vanishes.

properties even in a normal (nonsuperconducting) state. In setup (a) $t_\perp$ plays a significant and constructive role by facilitating the pathway through the flake, and one expects that if we could switch it off the current would vanish and transport through the BG regions is not possible. This could explain why the supercurrent in device (a) is much smaller than device (b), since the electrons must change the layer and enter another transport channel. However, in setup (b) the interlayer hopping acts only as a barrier for the movement of quasiparticles, and it somehow provides a resistance against transmission through the scattering region. In fact, in this case only the bottom ML is responsible for the transport, and consequently, varying none of the parameters, such as vertical bias, temperature, and doping, leads to a qualitative change in the supercurrent behavior and $0 - \pi$ transitions cannot take place. In other words, the upper layer of the flake only introduces an extra channel for scattering off the bottom layer, which slightly suppresses the electron transport through the system. When V_0 is absent, device (b) shows large transmission probabilities and as a result, the CPR is strongly nonsinusoidal, while increasing the vertical bias, which opens a gap in the band structure, leads to a decline in the supercurrent and CPR becomes closer to sinusoidal behavior.

In the remainder we will concentrate on the first device to understand the underlying physics of supercurrent reversal and $0 - \pi$ transitions which can occur by varying V_0 and μ of the BG flake, as well as temperature and the junction length when either V_0 or μ have a finite value. We present the dependence of the critical current I_c/I_0 on the temperature, varying the vertical bias scaled by the superconducting gap V_0/Δ_0 in Fig. 3. When no vertical bias voltage is applied, the junction remains always in π state for all temperatures below the critical temperature $T < T_c$. Nevertheless, applying V_0 the supercurrent as a function of T/T_c shows one cusp, indicating a π-to-0 transition. Moreover, the position of the cusps varies with V_0, and after $V_0 \sim 1.5\Delta_0$ the junction will be completely in 0 state, irrespective of the temperature variations. As one can see from Fig. 3, while at small values of vertical bias the critical current shows an overall decline, when it enters the 0 state for a wide range of temperatures, I_c can even increase with T.

In order to understand above-mentioned features, especially the mechanism of supercurrent reversal, we use the intuition based on the scattering matrix for the normal transport governed by S_B, which contains the properties of the BG flake contacted by MG regions. We have already discussed that the transmission through junction (a) is very small, and subsequently, the Andreev bound states are formed from single scatterings from the junction and the multiple scattering processes are strongly suppressed. Upon the electron-hole conversion or vice versa, at the NS interfaces the quasiparticles acquire an energy-dependent Andreev phase beside the superconducting phase $\pm\phi/2$. Moreover, the excitations passing between two interfaces may find an extra phase shift γ_{sc}, corresponding to the phase factors of the transmission coefficients t'_{12} and t_{21} defined by $t = |t| \exp(\gamma_{sc})$. Therefore one can convince oneself that the phase accumulated in the excitations during scattering γ_{sc} is added to the superconducting phase difference, which leads to a shift in the ϕ dependence of the ABS energies. The occurrence of a π state for the device (a) when $\mu = V_0 = 0$ signals that there must be some phase shift of amount π originating from γ_{sc}, while in the other setup there is no phase shift. The phase γ_{sc} in setup (a), in fact, originates from the transmission between lower and upper layers of the BG flake accompanied with the change of sublattice index $A_1 \to B_2$. To understand its root, let us have a look at the Hamiltonian (11) in which the two Dirac blocks, corresponding to the two MLs constructing the bilayer, differ with each other. The difference comes from the fact that we have AB stacking and the upper layer is $\pi/3$ rotated with respect to the lower. Subsequently, the wave-function spinor structures in two layers are not the same, which leads to the emergence of an extra phase γ_{sc} when the electrons need to pass from the lower to the upper layer. At this point one may wonder how the two setups become different, since in both of them the excitations undergo transitions between the layers several times depending on the length d. But as one can immediately see from Fig. 1 in the second setup, since at the end quasiparticles again leave the flake to the lower ML and we have the same number of passings from lower to the upper and vice versa, there will be no net phase accumulated in the transmission coefficients. On the other hand, in setup (a) there is always one more transition from the lower to the upper layer and the scattered excitations from the junction will have a net phase factor. It must be mentioned that γ_{sc} generally depends on the angle of incidence of the particles, as well as the doping μ and bias V_0. Thus in the absence of the bias and doping, the two setups are in π and 0 states, respectively, as the overall effect of scattering phases γ_{sc}. Note that if we had an AA stacked bilayer flake even in the first setup no phase factor appears due to the transition between the layers and subsequently the junction will be in the 0 state.

We have already seen that when a vertical bias is applied, the junction undergoes a π-to-0 transition, which is clear

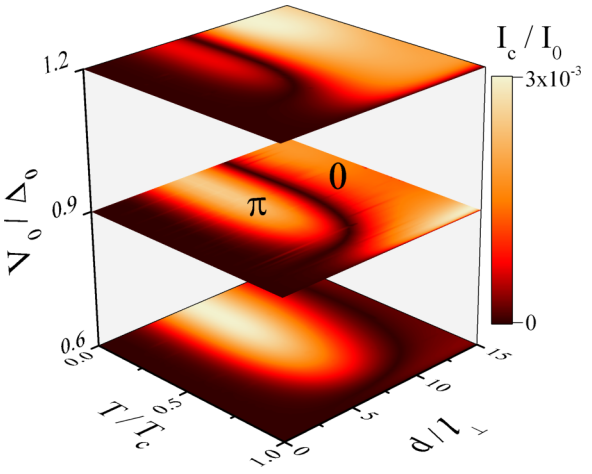

FIG. 4. (Color online) Critical current I_c/I_0 versus normalized temperature T/T_c and the normalized length of the junction $d/l_\perp$ are plotted for scaled bias values [0.6, 0.9, 1.2]. Two different states are labeled by π and 0.

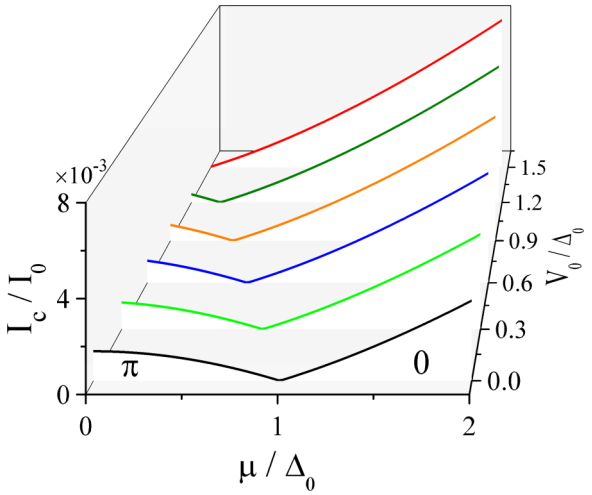

FIG. 5. (Color online) Critical current I_c/I_0 as a function of scaled doping of the BG flake μ/Δ_0 is demonstrated versus different values of scaled bias voltage $V_0/t_\perp$, shifted on the z axis, for setup (a) at zero temperature $T = 0$. The dimensionless length of the junction is $d/l_\perp = 4$. The cusp in the curves indicates the $\pi - 0$ transition.

from both Figs. 2 and 3. Until now we have considered a junction with fixed length $d/l_\perp \sim 4$, but if we increase the length as shown in Fig. 4, the Josephson current changes to a 0 state in a certain length which depends on the strength of the vertical bias and the temperature. Moreover, at the higher V_0 the domain of the π junction versus T/T_c and $d/l_\perp$ shrinks and becomes smaller. The bias-induced transition originates from the dependence of the scattering phase γ_{sc} to V_0. In fact, application of the bias between the layers leads to an asymmetry which influences the scattering processes and the phase of the different modes' transmission coefficients such that after a certain value of the vertical bias, depending on the length, the junction becomes 0 type. It must be noted that when the vertical bias voltage goes beyond the superconducting gap, the excitations carrying the supercurrent become evanescent due to the gap formation in the spectrum of the BG flake.

The effect of doping is somehow similar to the application of V_0 and leads to the $\pi - 0$ transitions, as indicated in Fig. 5. For small values of bias and doping in comparison with the superconducting gap, the junction remains in the π state, while when either μ or V_0 proceed well above Δ_0, the supercurrent shows a 0 behavior. In this state the critical current becomes larger upon increasing any of them. We can relate the transition with μ to the fact that by increasing the doping, more modes with different incidence angles participate effectively in transport and therefore their scattering phases γ_{sc} are washed out. This causes the junction to enter a 0 state but due to a mechanism different from the bias-induced 0 state.

We now comment on the possible experimental realization of the device under consideration and the predicted results. As mentioned in the Introduction, the steplike ML/BL interfaces and bilayer flakes connected to monolayer regions have already been observed and some transport experiments have been done based on them. On the other hand, there are many experiments on the superconducting proximity effect and Josephson junctions based on graphene. So it seems that the device we propose here is completely reliable in the current experimental setups and the supercurrent reversal can be investigated in them by applying the vertical bias voltage, changing the doping and even the temperature.

Another point we should discuss is regarding the validity of the present model beyond the approximation schemes that are used here. As discussed by Brey and Fertig, the continuum model based on the Dirac Hamiltonian for the nanoribbons of graphene has very good agreement with those obtained from the full tight-binding model, provided by the proper boundary conditions imposed to the continuous model [59]. Prior works on the BG flakes have proven the validity of continuum models, even for very short flakes of the order of a few nanometers [17–19]. Moreover, it must be noted that here we are considering flakes which are very wide, and their typical length is large in comparison with the effective length scale $l_\perp \sim 1$ nm. On the other hand, one may wonder about the effect of additional hopping terms in Eq. (11), like the interlayer coupling between the nondimer B and A sites, denoted by γ_3, on the results. It is known that such additional hoppings influence only the very-low-energy excitations and therefore do not affect the eigenstates and the corresponding pseudospins at sufficiently large energies [60,61]. As a result, when either the gap induced by the vertical bias or the doping is finite, the effect of γ_3 that leads to the trigonal warping is ignorable [62,63]. Although it may cause a small variation in the results, the qualitative behavior of the $0 - \pi$ transition which originates from the scattering phase γ_{sc} will be robust against the inclusion of higher-order hopping terms. Finally, we should emphasize that even without a self-consistent solution for the superconducting gap, the calculated Josephson currents are correct both qualitatively and quantitatively, whereas the superconducting gap is not affected by the low-doped normal region via an inverse proximity effect, which become even weaker in the short junction limit.

We close this discussion by comparing the $0 - \pi$ transition in our model and the conventional SFS type of junctions. The

predicted transition between 0 and π phases of the junction is always a single oscillation, as indicated in Fig. 5, in contrast to the conventional $0-\pi$ transitions in ferromagnetic-based junctions in which the critical current undergoes a series of oscillations as the signature of transitions. More importantly, the supercurrent reversal here has an entirely different origin compared to the conventional ferromagnetic Josephson junctions, where the spin degree of freedom plays the key role in several aspects. We argue that the scattering processes, accompanied by layer and sublattice index change, give rise to the phase γ_{sc} which is responsible for the supercurrent reversal, while in the SFS junctions the underlying mechanism is related to the spin splitting of Andreev bound states. Thus the origin of transitions in the two cases are very different, without any correlation between them.

IV. CONCLUSION

In this paper we employ scattering theory to study the supercurrent flowing through a weak link containing a biased BG flake embedded between two MG-based superconducting reservoirs. We investigate two possible configurations for the setup regarding how the BG flake is attached to the MG regions in the left and right. The reservoirs are connected either to different layers of the BG flake or to the same layer of the BG. The supercurrent passing through the undoped BG flake in the first situation is in the π state while the other shows a 0 behavior in the absence of the bias voltage ($V_0 = 0$). Both states are robust against varying the length of the junction d as well as the temperature T as long as $\mu = V_0 = 0$. We argue that the underlying mechanism of supercurrent reversal, characterized by the cusp in the critical current curves in the first setup, is related to the scattering phases accumulated in excitations upon transmission through the junction. We reveal that the biased BG flake in the second setup remains always in 0 state and increasing the vertical bias only suppresses the current. Nevertheless, the biased junction in the first setup undergoes a $\pi - 0$ transition at zero doping, provided by a finite value of V_0 depending on the length. Increasing the doping causes $\pi - 0$ transitions as well, so that the junction is in π state as long as μ and V_0 are small.

ACKNOWLEDGMENTS

We are grateful to Boris Altshuler and Yuli Nazarov for useful discussions. B.Z.R. thanks Gerrit Bauer for the hospitality and support during his visit to the Kavli Institute of NanoScience, Delft University of Technology in Delft. A.G.M. acknowledges financial support from Iran's Vice-Presidency for Science and Technology.

[1] A. K. Geim and K. S. Novoselov, Nat. Mater. **6**, 183 (2007).
[2] A. H. Castro Neto, F. Guinea, N. M. R. Peres, K. S. Novoselov, and A. K. Geim, Rev. Mod. Phys. **81**, 109 (2009).
[3] K. S. Novoselov, E. McCann, S. V. Morozov, V. I. Fal'ko, M. I. Katsnelson, D. Zeitler, U. Jiang, F. Schedin, and A. K. Geim, Nat. Phys. **2**, 177 (2006).
[4] E. McCann, D. S. Abergel, and V. I. Fal'ko, Solid State Commun. **143**, 110 (2007).
[5] E. McCann and M. Koshino, Rep. Prog. Phys. **76**, 056503 (2013).
[6] M. I. Katsnelson, K. S. Novoselov, and A. K. Geim, Nat. Phys. **2**, 620 (2006).
[7] T. Ohta, A. Bostwick, T. Seyller, K. Horn, and E. Rotenberg, Science **313**, 951 (2006).
[8] E. V. Castro, K. S. Novoselov, S. V. Morozov, N. M. R. Peres, J. M. B. Lopes dos Santos, J. Nilsson, F. Guinea, A. K. Geim, and A. H. Castro Neto, Phys. Rev. Lett. **99**, 216802 (2007).
[9] Y. Zhang, T.-T. Tang, C. Girit, Z. Hao, M. C. Martin, A. Zettl, M. F. Crommie, Y. R. Shen, and F. Wang, Nature (London) **459**, 820 (2009).
[10] J. B. Oostinga, H. B. Heersche, X. Liu, A. F. Morpurgo, and L. M. K. Vandersypen, Nat. Mater. **7**, 151 (2008).
[11] E. McCann, Phys. Rev. B **74**, 161403 (2006).
[12] H. Min, B. Sahu, S. K. Banerjee, and A. H. MacDonald, Phys. Rev. B **75**, 155115 (2007).
[13] S.-H. Ji, J. B. Hannon, R. M. Tromp, V. Perebeinos, J. Tersoff, and F. M. Ross, Nat. Mater. **11**, 114 (2012).
[14] F. Giannazzo, I. Deretzis, A. La Magna, F. Roccaforte, and R. Yakimova, Phys. Rev. B **86**, 235422 (2012).
[15] K. W. Clark, X.-G. Zhang, G. Gu, J. Park, G. He, R. M. Feenstra, and A.-P. Li, Phys. Rev. X **4**, 011021 (2014).
[16] J. Nilsson, A. H. Castro Neto, F. Guinea, and N. M. R. Peres, Phys. Rev. B **76**, 165416 (2007).
[17] T. Nakanishi, M. Koshino, and T. Ando, Phys. Rev. B **82**, 125428 (2010).
[18] T. Nakanishi, M. Koshino, and T. Ando, J. Phys.: Conf. Ser. **302**, 012021 (2011).
[19] M. Koshino, T. Nakanishi, and T. Ando, Phys. Rev. B **82**, 205436 (2010).
[20] J. Tian, Y. Jiang, I. Childres, H. Cao, J. Hu, and Y. P. Chen, Phys. Rev. B **88**, 125410 (2013).
[21] C. P. Puls, N. E. Staley, and Y. Liu, Phys. Rev. B **79**, 235415 (2009).
[22] W. Yan, S.-Y. Li, L.-J. Yin, J.-B. Qiao, J.-C. Nie, and L. He, arXiv:1502.00785.
[23] Y. Hasegawa and M. Kohmoto, Phys. Rev. B **85**, 125430 (2012).
[24] Z. Xiang Hu and W. Ding, Phys. Lett. A **376**, 610 (2012).
[25] H. Li, H. Li, Y. Zheng, and J. Niu, Phys. B (Amsterdam, Neth.) **406**, 1385 (2011).
[26] D. Yin, W. Liu, X. Li, L. Geng, X. Wang, and P. Huai, Appl. Phys. Lett. **103**, 173519 (2013).
[27] Y. Wang, J. Appl. Phys. **116**, 164317 (2014).
[28] M. Berahman, M. Sanaee, and R. Ghayour, Carbon **75**, 411 (2014).
[29] D. Dragoman, J. Appl. Phys. **113**, 214312 (2013).
[30] J. W. González, H. Santos, M. Pacheco, L. Chico, and L. Brey, Phys. Rev. B **81**, 195406 (2010).
[31] C. W. J. Beenakker, Phys. Rev. Lett. **97**, 067007 (2006).
[32] C. W. J. Beenakker, Rev. Mod. Phys. **80**, 1337 (2008).
[33] H. B. Heersche, P. Jarillo-Herrero, J. B. Oostinga, L. M. K. Vandersypen, and A. F. Morpurgo, Nature (London) **446**, 56 (2007).

[34] M. Titov and C. W. J. Beenakker, Phys. Rev. B **74**, 041401 (2006).
[35] A. G. Moghaddam and M. Zareyan, Phys. Rev. B **74**, 241403 (2006).
[36] D. Rainis, F. Taddei, F. Dolcini, M. Polini, and R. Fazio, Phys. Rev. B **79**, 115131 (2009).
[37] J. Linder and A. Sudbø, Phys. Rev. Lett. **99**, 147001 (2007).
[38] J. Linder, A. M. Black-Schaffer, T. Yokoyama, S. Doniach, and A. Sudbø, Phys. Rev. B **80**, 094522 (2009).
[39] A. M. Black-Schaffer and S. Doniach, Phys. Rev. B **78**, 024504 (2008).
[40] W. J. Herrera, P. Burset, and A. L. Yeyati, J. Phys.: Condens. Matter **22**, 275304 (2010).
[41] M. Alidoust and J. Linder, Phys. Rev. B **84**, 035407 (2011).
[42] W. A. Muñoz, L. Covaci, and F. M. Peeters, Phys. Rev. B **86**, 184505 (2012).
[43] C. Ojeda-Aristizabal, M. Ferrier, S. Guéron, and H. Bouchiat, Phys. Rev. B **79**, 165436 (2009).
[44] C. Girit, V. Bouchiat, O. Naaman, Y. Zhang, M. F. Crommie, A. Zettl, and I. Siddiqi, Nano Lett. **9**, 198 (2009).
[45] T. Dirks, T. L. Hughes, S. Lal, B. Uchoa, Y.-F. Chen, C. Chialvo, P. M. Goldbart, and N. Mason, Nat. Phys. **7** (2011).
[46] D. Jeong, J.-H. Choi, G.-H. Lee, S. Jo, Y.-J. Doh, and H.-J. Lee, Phys. Rev. B **83**, 094503 (2011).
[47] G.-H. Lee, D. Jeong, J.-H. Choi, Y.-J. Doh, and H.-J. Lee, Phys. Rev. Lett. **107**, 146605 (2011).
[48] G.-H. Lee, S. Kim, S.-H. Jhi, and H.-J. Lee, Nat. Commun. **6**, 6181 (2015).
[49] Q. Zhang, D. Fu, B. Wang, R. Zhang, and D. Y. Xing, Phys. Rev. Lett. **101**, 047005 (2008).
[50] C. Bai, Y. Yang, and X. Zhang, Appl. Phys. Lett. **92**, 102513 (2008).
[51] S.-G. Cheng, Y. Xing, J. Wang, and Q.-F. Sun, Phys. Rev. Lett. **103**, 167003 (2009).
[52] J. Schelter, B. Trauzettel, and P. Recher, Phys. Rev. Lett. **108**, 106603 (2012).
[53] J. Linder, T. Yokoyama, D. Huertas-Hernando, and A. Sudbø, Phys. Rev. Lett. **100**, 187004 (2008).
[54] A. G. Moghaddam and M. Zareyan, Phys. Rev. B **78**, 115413 (2008).
[55] Y. Asano, T. Yoshida, Y. Tanaka, and A. A. Golubov, Phys. Rev. B **78**, 014514 (2008).
[56] A. G. Moghaddam and M. Zareyan, Solid State Commun. **149**, 1106 (2009).
[57] B. Z. Rameshti, A. G. Moghaddam, and M. Zareyan, Europhys. Lett. **108**, 37002 (2014).
[58] D. Valencia, J.-Q. Lu, J. Wu, F. Liu, F. Zhai, and Y.-J. Jiang, AIP Adv. **3**, 102125 (2013).
[59] L. Brey and H. A. Fertig, Phys. Rev. B **73**, 235411 (2006).
[60] E. McCann and V. I. Fal'ko, Phys. Rev. Lett. **96**, 086805 (2006).
[61] A. G. Moghaddam and M. Zareyan, Phys. Rev. B **79**, 073401 (2009).
[62] I. Snyman and C. W. J. Beenakker, Phys. Rev. B **75**, 045322 (2007).
[63] L. M. Malard, J. Nilsson, D. C. Elias, J. C. Brant, F. Plentz, E. S. Alves, A. H. Castro Neto, and M. A. Pimenta, Phys. Rev. B **76**, 201401 (2007).